JACS
JOURNAL OF THE AMERICAN CHEMICAL SOCIETY

Communication

pubs.acs.org/JACS

Controlled Nucleation and Growth of DNA Tile Arrays within Prescribed DNA Origami Frames and Their Dynamics

Wei Li, Yang Yang, Shuoxing Jiang, Hao Yan, and Yan Liu*

Department of Chemistry and Biochemistry, and Center for Molecular Design and Biomimicry, Biodesign Institute, Arizona State University, Tempe, Arizona 85287, United States

Supporting Information

ABSTRACT: Controlled nucleation of nanoscale building blocks by geometrically defined seeds implanted in DNA nanoscaffolds represents a unique strategy to study and understand the dynamic processes of molecular self-assembly. Here we utilize a two-dimensional DNA origami frame with a hollow interior and selectively positioned DNA hybridization seeds to control the self-assembly of DNA tile building blocks, where the small DNA tiles are directed to fill the interior of the frame through prescribed sticky end interactions. This design facilitates the construction of DNA origami/array hybrids that adopt the overall shape and dimensions of the origami frame, forming a 2D array in the core consisting of a large number of simple repeating DNA tiles. The formation of the origami/array hybrid was characterized with atomic force microscopy, and the nucleation dynamics were monitored by serial AFM scanning and fluorescence spectroscopy, which revealed faster kinetics of growth within the frame as compared to growth without the presence of a frame. Our study provides insight into the fundamental behavior of DNA-based self-assembling systems.

DNA tiles composed of a small number of short synthetic DNA oligomers have been employed as building blocks for the assembly of two-dimensional (2D) and three-dimensional (3D) nanostructures.[1] Numerous current and potential applications of these DNA nanostructures have been demonstrated in biosensing, nanoelectronics, and molecular programming.[2] 2D assemblies of repeating DNA tiles with designed sticky ends (single-stranded overhangs) can grow into large arrays that reach micrometer to sub-millimeter scales.[1c,3] However, the lack of a defined boundary renders the 2D arrays of DNA tiles less than adequate when precise size control is desired.

DNA origami[1b,4] typically consists of one long, single-stranded DNA scaffold (e.g., a viral genome) and many (~200) short staple strands with designed sequences that hybridize to different parts of the scaffold and direct it to form a desired shape. Intrinsically, DNA origami structures have well-defined shapes and dimensions. Other non-repeating, scaffold-less DNA nanostructures[5] can be designed with precise size and shape control. However, these methods require hundreds or even thousands of unique DNA strands to reach structures on the 100 nm size scale. Expanding the size of DNA origami without sacrificing assembly yield and cost is an ongoing problem.[6] Here we utilize a hollow 2D DNA origami structure as a frame to direct the assembly of a 2D array of double-crossover (DX) tiles with high assembly yields and fixed dimensions, and at the same time investigate how controlled nucleation of DNA tiles can be used to improve our understanding of the dynamic process of DNA self-assembly. This hybrid structure integrates the advantages of fixed dimensions from DNA origami and large array size from repeating DNA tiles.

The 2D array we utilized is composed of four unique DX tiles (Figures 1A and S1). Each tile has a length of four full helical turns (42 base pairs), which is ~13.6 nm. The four sticky ends displayed from each tile are specifically designed to be complementary to one another so that the four tiles spontaneously self-assemble into a 2D array when mixed together, as illustrated in Figure 1C.

The DNA origami designed here consists of two distinct scaffold strands, using ssDNA from M13mp18 (7249 nucleotides long) and phi X 174 (5286 nucleotides long) (Figures 1B and S3). By combining the two scaffolds within a single structure we were able to significantly increase the size of the origami frame (~73% larger than origami structures assembled from M13mp18 DNA alone), such that a relatively large number of DX tiles could be incorporated into the DNA origami. However, larger structures have a tendency to suffer from slow assembly rates and result in low yields. To overcome these difficulties we maximized the contact between the two scaffolds that compose the frame. We assumed this strategy would increase the probability of effective cooperative assembly between the two long scaffold strands.[6a,b] To demonstrate that the growth of the 2D array within the origami frame can be directed asymmetrically, the frame was designed with one half wider than the other half (resembling an L-shape).

At several locations along the inner face of the top and bottom edges of the origami we pre-positioned 42 base-pairs long DNA duplexes linked to the frame through two crossovers (the same size as half of a DX tile). Both ends of these duplexes displayed a sticky end, with an intermolecular distance equal to the length of a DX tile. Besides these sticky ends along the top and bottom edges, the inner face of each of the DNA helices comprising the origami frame displayed a pair of sticky ends with designed sequences. When the origami frame and small DX tiles are mixed, the sticky ends along the inner edges of the frame serve as nucleation sites for the growth of a 2D array within the origami structure (Figure 1C). The specific sequences of the sticky ends

Received: November 9, 2013
Published: February 27, 2014

   dx.doi.org/10.1021/ja411446q | J. Am. Chem. Soc. 2014, 136, 3724−3727

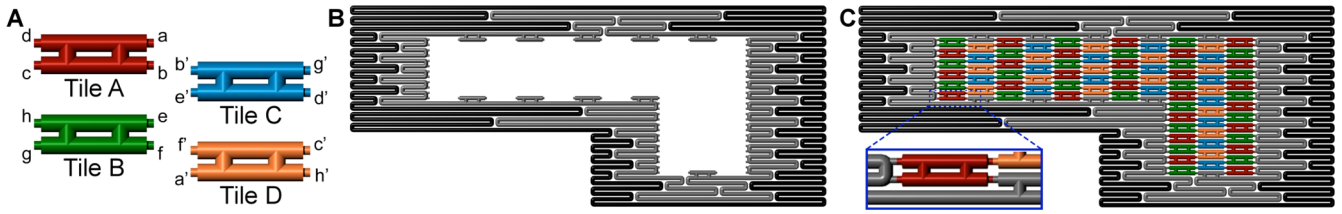

Figure 1. Seeded assembly of a 2D DX tile array within a DNA origami frame of fixed size. (A) The four unique DX tiles employed to assemble the 2D array. Each tile is four full helical turns along the helical axes. Unique sticky ends on tiles A and B are denoted as a–h. The complementary sticky ends on tiles C and D are denoted as a′–h′, respectively. (B) The origami frame structure. The origami frame is 210 nm long along the helical axis. The wider edge is 95 nm. The narrower edge is 60 nm. The hollow interior is 150 nm long and 15 or 32 nm wide. Sticky ends are located along the inner edges to initiate and direct the nucleation of DX tiles within the frame. The origami frame is scaffolded by two different single strands: M13mp18, which is shown in black, and phi X 174, which is shown in gray. (C) The origami frame directed assembly of a 2D array of DX tiles. The origami frame is designed to accommodate 82 DX tiles. The sticky ends displayed from the origami frame only associate with tile A or tile B, so that nucleation begins with tiles A and B (but not with tile C or D). The tiles are arranged in alternating columns of tiles A and B, and tiles C and D, respectively. The inset in C shows the tile–origami and tile–tile connections.

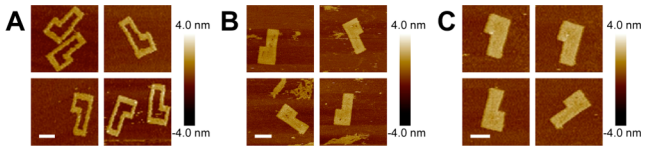

Figure 2. AFM images of the DNA origami frame and the frame/DX tile array hybrid. (A) Empty DNA origami frame. (B) Origami frame/array hybrid, after purification by agarose gel electrophoresis. (C) Origami frame/array hybrid purified by biotin mono-avidin bead interaction. The scale bars in the three figures are 100 nm.

facilitate the association of either tile A or tile B, starting from the inner corners (with three sticky end interactions required to realize each tile attachment) and along the inner edges of the frame (with two sticky end interactions required for each tile attachment). After one tile A and one tile B from consecutive rows are securely positioned, the sticky ends displayed from the two tiles work cooperatively to bind either tile C or tile D. As the nucleation and growth process continue, the origami frame is gradually filled by a 2D array of DX tiles (Figure 1C).

Methods for preparation and purification of the DNA origami frame can be found in Supporting Information. Formation of the origami frame was confirmed by atomic force microscopy (AFM) (Figure 2A). The origami frame formed well, as designed in Figure 1B. Since the two scaffold strands are in contact with one another in several places, there is a chance that more than one of each scaffold could be linked together to form larger aggregates with ill-defined shapes (Figure S4). Increasing the molar ratio between the helper strands and the scaffold strands helped to reduce the occurrence of aggregation. With a 30-fold excess of helper strands, the formation yield of the origami frame is ~70%, as evidenced by the AFM images.

The four unique DX tiles were prepared separately by annealing the respective strands mixtures (five strands each) from 90 to 4 °C over 2 h. When the tiles are mixed in the absence of the origami frame structure, they form 2D arrays of various sizes and unregulated boundaries (Figure S5).

The DNA origami frame-directed assembly of a 2D array of DX tiles was achieved by mixing the origami frame with tiles A–D. As shown in Figure 1C, the assembly ratio of each of the individual tiles to the origami frame varied from 16:1 to 25:1. Considering the possibility of spontaneous formation of "unframed" 2D arrays that were not initiated and directed by the origami structure, all tiles were mixed with the origami frame at a molar ratio of 100:1. This high ratio of DX tiles to origami ensures the existence of a large excess of tiles in solution. Next, the tile and origami frame mixture was incubated at 25 °C overnight. Finally, the origami frame/2D array hybrid was purified by agarose gel electrophoresis to remove the excess free DX tiles and "unframed" tile arrays (Figure S6). The band corresponding to the framed arrays was cut and extracted from the gel and then characterized by AFM (Figure 2B). The AFM images show that the DX tiles assembled within the origami frame as designed. Approximately 70% of the origami frames were fully filled by the 2D array without any deformation. Most of the defective frame/array hybrids were grown in deformed frames. Only a few were incompletely filled.

The frame/array hybrids cannot be sufficiently separated from the frame-free 2D arrays using agarose gel electrophoresis (Figure S7) due to their similarity in size. To obtain a cleaner separation, the origami frame was modified by covalently labeling one staple strand with a biotin, and subsequently separated from the frame-free 2D arrays and individual tiles using monomeric avidin resin (Thermo Scientific). The AFM images show that the frame/array hybrids purified by this method (Figure 2C) are well-formed, with fewer impurities visible in the background (Figure S8). Note that in Figure 2C, every origami frame has a bright spot at the inner corner position, which is the position of the biotin modification protruding from the origami surface. The yield and defects observed are similar to those purified by gel electrophoresis.

The sources of defects in the frame/array hybrids required careful examination (Figure S10). We propose that one major origin of the defects is "cross-talk" between the complementary sticky ends in different rows of the tile array. Because the inner corner positions of the frame each display three sticky ends for the tiles to attach to, and the positions along the inner edges each display two sticky ends, we envision that the first step of the self-assembly process is the association of the tiles at the inner corners of the frame, followed by association with the inner edges, effectively creating a new boundary layer. At the same time, this process exposes additional sticky ends that allow tiles in a second row (or column) to attach. It is at this stage, due to the flexibility of DX tiles at the crossover points, that two sticky ends on tiles in non-neighboring rows within the same column (with a gap the width of one or two tiles) may be able to hybridize to the corresponding sticky ends displayed from a single tile in the next column such that the frame shrinks in width and bends inward (thus, the frame/array hybrid would appear thinner). Similarly, but oppositely, there could be additional rows of tiles inserted, causing the frame/array hybrid to appear wider than designed.

dx.doi.org/10.1021/ja411446q | J. Am. Chem. Soc. 2014, 136, 3724–3727

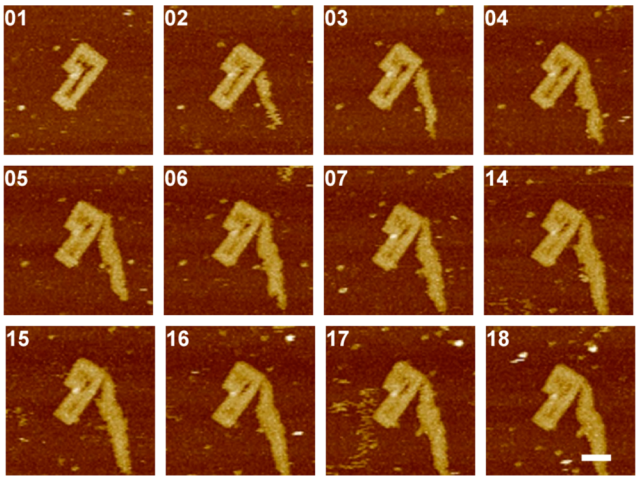

Figure 3. FS-AFM images showing the dynamic nucleation and growth of DX tiles within a DNA origami frame. As soon as the reactants are all deposited on the mica surface, scanning begins. The total scan time for each image is 87 s. Frames 8−13 are not shown because there was little change in the images during that time period. The scale bar is 100 nm.

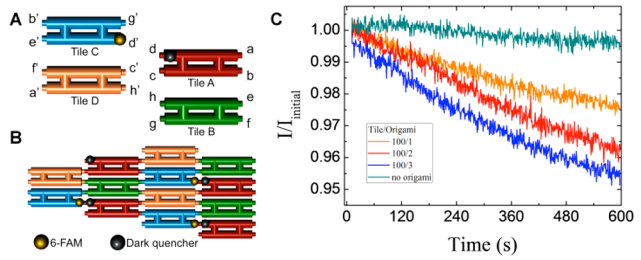

Figure 4. Nucleation kinetics monitored by fluorescence. (A) Tile C is modified with the fluorescence dye 6-FAM at sticky end d′. Tile A is modified with Iowa black dark quencher at sticky end d. Tiles B and D are not modified. (B) After assembly of the four tiles, either with or without the presence of the origami frame, the fluorescence dye is brought next to the dark quencher. The fluorescence intensity decreases as the self-assembly process proceeds. In panels A and B, the yellow dots represent 6-FAM, and the black dots represent the dark quencher. (C) Normalized fluorescence decrease. The normalization is achieved by dividing the fluorescence intensity by the initial intensity of each experiment. With the same amount of tiles present, the initial intensities in each experiment are the same. The cyan curve shows that without the presence of the origami seed, the nucleation exhibits a very slow rate. The orange, red, and blue curves show the reaction at origami concentrations of 0.2, 0.4, and 0.6 nM, respectively. The tile concentrations are 20 nM in all experiments.

To better understand the self-assembly of DX tiles within the DNA origami frame, the nucleation and growth processes were monitored using real-time AFM scanning which allows consecutive images of a liquid sample deposited on a mica surface to be collected. Each scan can be collected in a short time (<1 min per 516 × 516 pixel image) without compromising the image quality. First, the empty DNA origami frame, together with tiles C and D (in a ratio of 1:100:100, respectively) were deposited on mica. Because the sticky ends displayed from the frame are all designed to associate with tiles A and B but not tile C or tile D, and tiles C and D do not associate each other, the nucleation does not begin at this stage. Next, a mixture of tiles A and B (100-fold excess to the origami frame) were injected into the sample droplet. Nucleation is expected to begin immediately and continuous AFM imaging in the same area was initiated. Figure 3 shows the consecutive AFM images collected at constant intervals (87 s per image) that allowed us to monitor the dynamic self-assembly of the DX tiles within the origami frame. From the images, we observed that the nucleation of DX tiles starts in the direction parallel to the DNA helices along the inner edges, as well as in the direction perpendicular to the helices along the inner edges. We should point out that the excess tiles may undergo spontaneous nucleation in solution, and small sections of frame-free 2D arrays appear in the background, as first observed in the second image. It is possible that nucleation of the free array occurred before the array was deposited on the mica between imaging the first and second image. Regardless, the growth phase without the frame appears to occur more rapidly than within the frame, possibly due to fewer structural constrains. As the concentration of free DX tiles quickly decreases after nucleation, the growth of the tile array within the origami frame slows down significantly before the frame is completely filled. Nevertheless, the nucleation and growth process within the origami frame is finished within 1 h. The same process is expected to be faster in solution without the restriction of the surface.

While real-time AFM scanning permits direct observation of the nucleation process, it is likely that the mica surface restricts the ability of the tiles to enter the origami frame, thus making the nucleation kinetics different from that in solution. Thus, we modified one of the DX tiles with a fluorescent dye and a neighboring tile with a dark quencher, and studied the nucleation kinetics in solution by monitoring the change in fluorescence intensity of the dye with time. Specifically, the ssDNA comprising sticky end d′ on tile C was modified with 6-carboxyfluorescein (6-FAM), and the ssDNA comprising sticky end d on tile A was modified with an Iowa Black dark quencher (Figures 4A and S12A). Upon association of the four tiles within the 2D array (with and without the DNA origami frame) 6-FAM is brought into close proximity with the dark quencher, and its fluorescence intensity is expected to decrease as the assembly process proceeds (Figure 4B).

The fluorescence change with time was monitored using a fluorometer (λ_{ex} = 495 nm, λ_{em} = 520 nm), which reflects the kinetics of the tile−tile assembly process (Figure 4C, and additional data shown in Figure S12B). In Figure 4C, four curves are shown to represent four different experiments. The slowest decay represents the self-assembly of the four tiles in the absence of the origami frame. This very slow reaction rate indicates that the spontaneous nucleation process in solution is significantly slower than with a seed. The remaining three curves represent the reaction kinetics with varying molar ratios between each tile and the origami seed (100:1, 100:2, and 100:3, respectively). As expected, as the concentration of the nucleation seed increases, the initial rate of the reaction becomes higher.

The concentration of the origami seed and the DX tiles used for fast-scan AFM experiment were 4-fold lower than those used for fluorescence measurements. Thus, the spontaneous nucleation and growth rate observed in solution is apparently much slower than on the mica surface. The rapid emergence of seed-free nucleation in the FS-AFM image (Figure 3) may result from a surface-mediated process, where the mica may also act as a nucleation point, aiding the tile−tile assembly process.[7] For surface-mediated assembly on mica, with the exception of a short delay time (between image frames 1 and 2), the spontaneous nucleation and growth rate outside the frame seems comparable to the seeded nucleation and growth within the frame. Meanwhile, for the assembly process in solution, the seeded

dx.doi.org/10.1021/ja411446q | J. Am. Chem. Soc. 2014, 136, 3724−3727

nucleation and growth rate within the origami frame is much faster than the spontaneous nucleation and growth rate without the frame. This result indicates the importance of nucleation in the kinetics of tile array assembly.[8]

To characterize the kinetics of nucleation, we constructed a reaction model and calculated the reaction rate constant, k, from our data. The reaction rate between tile C and the origami frame can be expressed by

$$-\mathrm{d}[\mathrm{C}]/\mathrm{d}t = k[\mathrm{origami}][\mathrm{C}] \quad (1)$$

We assume that at the initial stages of seeded nucleation, the small number of tiles assembled inside the origami frame do not affect the accessibility or diffusion of the origami significantly, thus, we may treat the concentration of origami in eq 1 as a constant. At a certain time t, the concentration of unassembled tile C is

$$[\mathrm{C}]_t = [\mathrm{C}]_0\, \mathrm{e}^{-k[\mathrm{origami}]t} \quad (2)$$

This assumption fails when the origami is more thoroughly filled, which would change the properties of the frame and, thus, the reaction rate constant k. Therefore, we collected and analyzed the fluorescence change only in the early stages of the reaction (the first 10 min), where only a small percentage of the assembly process is complete.

The fluorescence intensity observed is the sum of the fluorescence intensities from the free and associated tile C, which are linear to the concentrations of each species:

$$I_t = a[\mathrm{C}]_t + b([\mathrm{C}]_0 - [\mathrm{C}]_t) = (a-b)[\mathrm{C}]_t + b[\mathrm{C}]_0 \quad (3)$$

Here, a and b are constants. We normalized the fluorescence intensity by dividing both sides of eq 3 by the initial intensity, $a[\mathrm{C}]_0$, and obtained

$$\frac{I_t}{I_{\mathrm{init}}} = \frac{a-b}{a[\mathrm{C}]_0}[\mathrm{C}]_t + \frac{b}{a} = \frac{a-b}{a}\mathrm{e}^{-k[\mathrm{origami}]t} + \frac{b}{a} \quad (4)$$

Therefore, a linear equation can be obtained:

$$\ln\left(\frac{I_t}{I_{\mathrm{init}}} - \frac{b}{a}\right) = -k[\mathrm{origami}]t + \ln\frac{a-b}{a} \quad (5)$$

The ratio b/a is experimentally measured as 0.399, which equals the ratio of the fluorescence intensity of the fully assembled structure of all four tiles, to that of individual tile C in the presence of the same concentration of tiles A and C. The data in Figures 4C and S12B were fit by eq 5, and the nucleation rate constant k obtained from the slope is $(2.3 \pm 0.4) \times 10^5\ \mathrm{M}^{-1}\cdot\mathrm{s}^{-1}$. We should note that we are experimentally monitoring the change of the occupancy status at one of the sticky ends on tile C (where the fluorescence dye is labeled). The nucleation sites for tile C in the origami frame must be first generated by the binding of tiles A and B first, and then regenerated by the self-assembly of other three tiles. Each regeneration cycle requires the attachment of three to five other tiles. Thus, the time that it takes for the attachment of a random individual tile in the origami frame is expected to be, on average, one-third to one-fifth of the nucleation time of tile C. Therefore, the nucleation rate constant for random tile association should be 3−5 times the value of constant k that we determined from our model. Considering this factor, the nucleation rate constant is on the same order of magnitude as $10^6\ \mathrm{M}^{-1}\cdot\mathrm{s}^{-1}$, consistent with values previously reported in the literature.[8]

In summary, we successfully utilized a large DNA origami frame to regulate the growth of a 2D array of DX DNA tiles with high yield. The dynamics of nucleation were monitored using real-time AFM and fluorescence kinetics. We obtained the nucleation rate constant of assembly with and without the presence of a DNA origami seed. The assembly of the frame/array hybrid structures takes advantage of the properties of DNA origami and 2D arrays such that the resulting structure has a defined shape and dimensions, with aperiodic peripheral sequences and a solid periodic core that consists of a small number of unique DNA sequences.[3a] Our approach will be useful and efficient to create DNA-based nanodevices when definite boundaries and exact numbers of addressable positions are required.

■ ASSOCIATED CONTENT

Supporting Information

Details of experimental methods, DNA sequences, and Figures S1−S11. This material is available free of charge via the Internet at http://pubs.acs.org.

■ AUTHOR INFORMATION

Corresponding Author

yan_liu@asu.edu

Notes

The authors declare no competing financial interest.

■ ACKNOWLEDGMENTS

This work was supported by grants from the Army Research Office, Office of Naval Research, National Science Foundation, Department of Energy, and National Institutes of Health to Y.L.

■ REFERENCES

(1) (a) Seeman, N. C. *J. Theor. Biol.* **1982**, *99*, 237. (b) Rothemund, P. W. K. *Nature* **2006**, *440*, 297. (c) Winfree, E.; Liu, F.; Wenzler, L. A.; Seeman, N. C. *Nature* **1998**, *394*, 539.

(2) (a) Seeman, N. C. *Nature* **2003**, *421*, 427. (b) Voigt, N. V.; Torring, T.; Rotaru, A.; Jacobsen, M. F.; Ravnsbaek, J. B.; Subramani, R.; Mamdouh, W.; Kjems, J.; Mokhir, A.; Besenbacher, F.; Gothelf, K. V. *Nat. Nanotechnol.* **2010**, *5*, 200. (c) Deng, Z.; Samanta, A.; Nangreave, J.; Yan, H.; Liu, Y. *J. Am. Chem. Soc.* **2012**, *134*, 17424. (d) Barish, R. D.; Schulman, R.; Rothemund, P. W. K.; Winfree, E. *Proc. Natl. Acad. Sci. U.S.A.* **2009**, *106*, 6054. (e) Qian, L. L.; Winfree, E. *Science* **2011**, *332*, 1196. (f) Li, W.; Yang, Y.; Yan, H.; Liu, Y. *Nano Lett.* **2013**, *13*, 2980.

(3) (a) Yan, H.; Park, S. H.; Finkelstein, G.; Reif, J. H.; LaBean, T. H. *Science* **2003**, *301*, 1882. (b) He, Y.; Chen, Y.; Liu, H.; Ribbe, A. E.; Mao, C. *J. Am. Chem. Soc.* **2005**, *127*, 12202.

(4) (a) Dietz, H.; Douglas, S. M.; Shih, W. M. *Science* **2009**, *325*, 725. (b) Han, D.; Pal, S.; Nangreave, J.; Deng, Z.; Liu, Y.; Yan, H. *Science* **2011**, *332*, 342.

(5) (a) Wei, B.; Dai, M.; Yin, P. *Nature* **2012**, *485*, 623. (b) Ke, Y.; Ong, L. L.; Shih, W. M.; Yin, P. *Science* **2012**, *338*, 1177.

(6) (a) Zhao, Z.; Liu, Y.; Yan, H. *Nano Lett.* **2011**, *11*, 2997. (b) Yang, Y.; Han, D.; Nangreave, J.; Liu, Y.; Yan, H. *ACS Nano* **2012**, *6*, 8209. (c) Pound, E.; Ashton, J. R.; Becerril, H. c. A.; Woolley, A. T. *Nano Lett.* **2009**, *9*, 4302. (d) Zhang, H.; Chao, J.; Pan, D.; Liu, H.; Huang, Q.; Fan, C. *Chem. Commun.* **2012**, *48*, 6405.

(7) (a) Sun, X.; Ko, S. H.; Zhang, C.; Ribbe, A. E.; Mao, C. *J. Am. Chem. Soc.* **2009**, *131*, 13248. (b) Lee, J.; Hamada, S.; Hwang, S. U.; Amin, R.; Son, J.; Dugasani, S. R.; Murata, S.; Park, S. H. *Sci. Rep.* **2013**, 3. (c) Hamada, S.; Murata, S. *Angew. Chem., Int. Ed.* **2009**, *48*, 6820.

(8) (a) Schulman, R.; Winfree, E. *Proc. Natl. Acad. Sci. U.S.A.* **2007**, *104*, 15236. (b) Pinheiro, A. V.; Nangreave, J.; Jiang, S.; Yan, H.; Liu, Y. *ACS Nano* **2012**, *6*, 5521.